J Mater Sci: Mater Med (2011) 22:2249–2259
DOI 10.1007/s10856-011-4416-2

Hydroxyapatite-anatase-carbon nanotube nanocomposite coatings fabricated by electrophoretic codeposition for biomedical applications

Bokai Zhang · Chi Tat Kwok

Received: 11 April 2011 / Accepted: 6 August 2011 / Published online: 18 August 2011

Abstract In order to eliminate micro-cracks in the monolithic hydroxyapatite (HA) and composite hydroxyapatite/carbon nanotube (HA/CNT) coatings, novel HA/TiO_2/CNT nanocomposite coatings on Ti6Al4V were attempted to fabricate by a single-step electrophoretic codeposition process for biomedical applications. The electrophoretically deposited layers with difference contents of HA, TiO_2 (anatase) and CNT nanoparticles were sintered at 800°C for densification with thickness of about 7–10 μm. A dense and crack-free coating was achieved with constituents of 85 wt% HA, 10 wt% TiO_2 and 5 wt% CNT. Open-circuit potential measurements and cyclic potentiodynamic polarization tests were used to investigate the electrochemical corrosion behavior of the coatings in vitro conditions (Hanks' solution at 37°C). The HA/TiO_2/CNT coatings possess higher corrosion resistance than that of the Ti6Al4V substrate as reflected by nobler open circuit potential and lower corrosion current density. In addition, the surface hardness and adhesion strength of the HA/TiO_2/CNT coatings are higher than that of the monolithic HA and HA/CNT coatings without compromising their apatite forming ability. The enhanced properties were attributed to the nanostructure of the coatings with the appropriate TiO_2 and CNT contents for eliminating micro-cracks and micro-pores.

B. Zhang · C. T. Kwok (✉)
Department of Electromechanical Engineering, Faculty of Science and Technology, University of Macau, Av. Padre Tomas Pereira, Taipa, Macau, China
e-mail: fstctk@umac.mo

1 Introduction

Titanium and its alloys are commonly employed as load-bearing orthopedic and dental implants because of their high mechanical strength and toughness, low density and excellent corrosion resistance in physiological environment [1]. However, the bio-inertness of the metallic surfaces inhibits the growth of bone tissue [2, 3]. In order to overcome this shortage, hydroxyapatite (HA, $Ca_{10}(PO_4)_6(OH)_2$) has been applied as a coating on the metallic implants due to its similarity in chemical compositions, high biocompatibility and osteoconductivity to bone tissue of human. Plasma spraying is currently the most extensively used manufacturing process for HA coatings on the metallic implants but long-term stability of plasma sprayed coatings could be a problem because of their high degree of porosities, poor bond strength, non-stoichiometric composition, non-uniformity and amorphous structure [4–6]. Moreover, plasma spraying requires the size of HA particles ranging from 20 to 40 μm and thus relatively thick coatings are formed. These thick coatings are likely to fracture during insertion and service and have unpredictable dissolution rates. In view of these shortcomings, other alternative methods such as dip coating, ion sputtering, sol–gel coating, pulsed-laser deposition, laser surface alloying, electron-beam deposition, biomimetic process and electrophoretic deposition (EPD) have been proposed to fabricate HA coatings [7]. Among the various fabrication methods, EPD is a promising technique, with merits including simple and low-cost apparatus, short processing time, easy control of thickness and capability of coating complex-shaped implants [8, 9]. In EPD, charged ceramic particles dispersed or suspended in a liquid medium are attracted and deposited onto a conductive metallic substrate of opposite charge on application of a DC electric field [8].

However, a subsequent sintering process is required to enhance densification of the HA coatings [9]. Owing to the mismatch of coefficients of thermal expansion of the HA coatings and the metallic substrates, sintering often causes residual stress, which leads to micro-cracks in the coatings [10], reduction in adhesion between them [11] and peeling of coatings.

Recent studies have reported that nano-structured HA coatings fabricated by EPD have high chemical homogeneity, reduced flaw size, microstructural uniformity, and lower sintering temperature for densification [12]. The nano-scale roughness and grains, and the high volume fraction of grain boundaries in nano-structured HA coatings can increase osteoblasts adhesion, proliferation, and mineralization [13]. Due to their extraordinary elastic modulus (200–1,000 GPa) and tensile strength (11–63 GPa), chemical stability and light-weight arising from the unique cylindrical graphite structure and small dimensions, carbon nanotubes (CNTs) have attracted attention as reinforcement in HA for forming nanocomposite coatings [14, 15]. According to the Hall–Petch principle, the smaller the particles reinforced in the coating, the more strengthened the coating will be [16]. Moreover, addition of CNTs is able to transfer and eliminate residual stress in the HA coating [17]. Some published papers reported the results on the HA coating reinforced with CNTs fabricated by EPD for enhancing adhesion strength, mechanical and corrosion properties [17–23]. It was shown that the addition of 1 wt% CNT in HA increased the hardness, elastic modulus and interlaminar shear strength of the HA/CNT composite layers [18]. Improvement in the mechanical performance of the HA/CNT coating was explained by inducing toughening mechanisms, that is, crack deflection [18–20]. Kaya and his coworkers also investigated the effect of CNT addition on the bonding strength of the electrophoretically deposited layer on Ti6Al4V [20]. After sintering at 600°C for 2 h under flowing nitrogen gas, the bonding strength for the HA/CNT composite coating containing 2 wt% CNT was higher than the one with 1 wt% CNT (2.76 and 1.84 MPa, respectively), while the bonding strength for the monolithic HA coating was only 0.7 MPa, in agreement with the results of Lin et al. [17]. Adding CNTs helps to prevent peeling of the HA/CNT coating by acting as reinforcement network [18]. However, thick coating achieved by long deposition time can lead to extensive surface micro-cracks after sintering due to thermal expansion mismatch between Ti6Al4V and HA/CNT coating [18]. In a previous study of the present authors, 10 μm thick composite coatings of HA with 4–25 wt% CNT on Ti6Al4V sintered at 800°C for 1 h were attempted to fabricate by EPD [23]. Among the coated specimens, the HA coating reinforced with 10 wt% CNT was reported to have the highest corrosion resistance in Hanks' solution. But the presence of micro-cracks in the HA/CNT coating led to low adhesion strength [23]. On the other hand, a nanostructured TiO_2 inner layer between Ti6Al4V substrate and outer HA coating formed by EPD was reported to be acting as a diffusion barrier for reducing HA decomposition due to ion migration from the substrate into the HA coating [24]. Nevertheless, increase in the voltage for TiO_2 deposition resulted in surface cracks and reduction in adhesion strength of HA/TiO_2 coating.

In order to lessen the micro-cracking problem and improve the adhesion strength of the monolithic HA and composite HA/CNT coatings, fabrication of HA/TiO_2/CNT nanocomposite coatings on Ti6Al4V with different contents of HA, TiO_2 and CNT nanoparticles were attempted by a single-step electrophoretic codeposition process in the present study. Surface characterization, corrosion behavior, hardness, adhesion strength and apatite-forming ability of the nanocomposite coatings on Ti6Al4V were also investigated.

2 Experimental details

2.1 Specimens preparation and characterization

As-received titanium alloy Ti6Al4V in form of cylindrical bar with a diameter of 13.5 mm was cut into discs with thickness of 10 mm. The discs were then successively ground with 200, 400, 600, 800-grit silicon carbide papers, washed with alcohol and dried in air. The nano-size coating materials were commercially obtained including needle-shaped HA powder with size of 50 × 200 nm (Kingo Co., China), multi-walled CNTs with an average diameter of 30 nm and length of 1 μm (Shenzhen Nanoport Co., China) and spherical TiO_2 powder with size of 10 nm (anatase, International Laboratory Ltd., USA). The blend of HA/TiO_2/CNT with three different weight percents and corresponding designations of the coatings are shown in Table 1. The monolithic HA and composite HA/CNT coatings without TiO_2 (designated as nHA and HA10CNT, respectively) on Ti6Al4V were also fabricated for comparison. In the previous study of the present authors, excessive CNTs (20–25 wt%) were found to result in incomplete infiltration of HA into the CNT network [23]. So 5–10 wt% CNTs were added to fabricate the specimens in the present study. The blend of HA/TiO_2/CNT (2.5 wt%) with the addition of a little benzalkonium chloride as a cationic surfactant [25] was ultrasonically mixed in anhydrous ethanol by a vibratory sonicator (Sonics VCX750, USA) at 20 kHz and 25°C for an hour to obtain a homogeneous colloidal suspension. In order to avoid severe oxidation of Ti6Al4V at high voltage, cathodic EPD was used for codeposition of HA/TiO_2/CNT nanoparticles on

the Ti6Al4V substrate. Ti6Al4V played the role of cathode and a graphite bar with dimensions of 7.5 × 11 × 85 mm^3 acted as the anode. 100 ml colloidal suspension of HA/TiO_2/CNT was put into a 250 ml beaker and continuously stirred by a magnetic stirrer. Both electrodes were immersed in the suspension and kept at a distance of 20 mm and 25°C, under a deposition voltage of 200 V for 10 s in order to achieve coating thickness of about 10 μm. High deposition voltage was used for achieving a faster deposition rate [26]. The nanoparticles in the suspension were positively charged to enable their migration towards the Ti6Al4V substrate (the cathode) under the applied electric field. The details mechanisms involved in electrophoretic codeposition of equally charged particles have been explained by considering the different trajectories of nanoparticles in suspension [27].

After EPD, HA/TiO_2/CNT layer was deposited on the surface of Ti6Al4V and allowed to dry in air at room temperature, and then put into a vacuum furnace (Centurion, QEX 9494306, USA) for sintering at 800°C and 3 Torr, at a heating rate of 100°C/h, a dwell time of 1 h, and a cooling rate of 100°C/h. Low sintering temperature below the α–β transition temperature of Ti6Al4V (955–1,010°C) was selected to avoid degradation of its mechanical properties [28] and avoid partial transformation of HA at 875°C into more soluble phases such as tricalcium phosphate (α-TCP or β-TCP) [29].

The coating thickness was evaluated by a coating thickness gauge (Elcometer 456, UK) and confirmed by cross-sectional observation. In addition to visual inspection of the overall macroscopic quality of the surface of coatings, scanning-electron microscope (SEM, Hitachi S3400N, Japan) and energy-dispersive spectrometer (EDS, Horiba EX-250, Japan) were used to examine the surface morphology and compositions of the coatings, respectively. A thin layer of gold with thickness of about 1 μm was coated on the specimens to increase conductivity by an ion sputter (Hitachi E1010, Japan). X-ray diffractometer (XRD, Bruker D8 Advance, Germany) was used to identify the crystalline phases present in the coatings. The XRD measurements were performed using a Cu-Kα X-ray source with a scanning rate of 0.025°/s and a scanning range of 20°–60°.

2.2 Corrosion study

To investigate the electrochemical corrosion behavior, the various uncoated and coated specimens was fixed in a flat cell (Princeton Applied Research K0235, USA) exposing an area of 0.34 cm^2 in Hanks' physiologic solution (0.14 g/l anhydrous $CaCl_2$, 0.1 g/l anhydrous $MgSO_4$, 0.4 g/l KCl, 0.06 g/l anhydrous KH_2PO_4, 8 g/l NaCl, 0.06 g/l anhydrous Na_2PHO_4, 0.35 g/l $NaHCO_3$, 1 g/l glucose, and 0.011 g/l Phenol Red). The solution was kept at 37 ± 1°C by an electronic water bath. Open-circuit potential (*OCP*) measurement and cyclic potentiodynamic polarization of the specimens were performed using a potentiostat (Princeton Applied Research VersastatII, USA). All potentials were measured with respect to a saturated calomel electrode (SCE, 0.244 V vs. SHE) as the reference electrode. A 2 × 2 cm^2 platinum net served as the counter electrode for current measurement. *OCP* was recorded for 10^4 s and then followed by cyclic polarization. For the cyclic polarization experiment, the potential was increased at a rate of 1 mV/s, starting from 200 mV below the *OCP* conforming to ASTM Standard G61-94 [30]. The scan was reversed when a current density of 5 mA/cm^2 was reached. From the polarization curve, the corrosion current density (I_{corr}) was determined by Tafel extrapolation with the aid of a commercial software (PowerCORR, V.2.42). Three specimens were used in the *OCP* measurement and cycle polarization. The steady *OCP* and I_{corr} with standard deviations were shown in Table 1.

2.3 Hardness and adhesion strength tests

Vickers hardness tests were performed on the surface of all coated specimens using a micro-hardness tester. A load of 9.8 N was applied with a dwell time of 10 s. The coated specimens were also undergone tensile adhesive strength test using a universal force testing machine (Chatillon, LCTM-500, USA) with a 2.5 kN load cell and a crosshead

Table 1 Compositions, corrosion parameters, average hardness and adhesion strength of uncoated and coated specimens

Designations of specimens	HA (wt%)	TiO_2 (wt%)	CNT (wt%)	*OCP* (V)	I_{corr} (μA/cm^2)	Average hardness (HV)	Adhesion strength (MPa)
Ti6Al4V	–	–	–	−0.306 ± 0.00076	8.00 ± 0.013	421 ± 8.2	–
nHA	100	0	0	0.130 ± 0.00043	1.66 ± 0.045	585 ± 12.6	5.9 ± 0.44
nHA10CNT	90	0	10	−0.020 ± 0.00043	0.15 ± 0.047	923 ± 16.4	6.5 ± 0.55
nHA5TiO5CNT	90	5	5	−0.002 ± 0.00041	0.12 ± 0.044	880 ± 18.8	6.4 ± 0.68
nHA5TiO10CNT	85	5	10	−0.031 ± 0.00051	0.089 ± 0.037	956 ± 14.0	11.9 ± 0.79
nHA10TiO5CNT	85	10	5	0.096 ± 0.00047	0.084 ± 0.035	991 ± 19.4	12.6 ± 0.73

speed of 5.0 mm/min, conforming to International Standard ISO 13779-4:2002(E) [31]. Adhesion strength of the coating was determined by applying a uniaxial tensile load to a cylindrical test assembly composed of the coated specimen bonded to an uncoated Ti6Al4V both with diameter of 13.5 mm. The parts of the test assembly were bonded together by epoxy adhesive and cured at room temperature for 24 h prior to the adhesion strength test. The adhesion strength was calculated as the load at failure divided by the coated area bonded to the stub. Four coated specimens were used in the hardness and adhesion tests and the average hardness and adhesion strength with standard deviations were shown in Table 1.

2.4 In vitro bioactivity test

The uncoated and coated Ti6Al4V were immersed in 500 ml of Hanks' physiologic solution at 37°C for 4 weeks to study the ability of the coating to induce apatite films on their surface. In order to avoid depositing of apatite on the surface of the coatings by gravity, the specimens were vertically suspended in a sealed polyethylene jar. The specimens were taken out after 4 weeks, washed with distilled water and dried at room temperature for subsequent SEM analysis.

3 Results and discussion

3.1 Characterization of the coatings

The surface morphologies of the coated specimens are shown in Fig. 1. From Fig. 1a–c, the specimens nHA, nHA10CNT and nHA5TiO5CNT show extensive micro-cracks on the surface (indicated by red arrows), nHA5TiO10CNT has fewer cracks (Fig. 1d-i), while no crack is observed on the surface of nHA10TiO5CNT (Fig. 1e-i). Wei and his co-workers reported that the less equiaxed HA particles such as needle-like and plate-like ones have higher cracking susceptibility in the electrophoretically deposited coatings after sintering than the round HA particles [32]. In addition, the difference in thermal expansion coefficients of HA ($15.2 \times 10^{-6}°C^{-1}$) and Ti6Al4V ($8.6 \times 10^{-6}°C^{-1}$) would lead to excessive strain and hence forming micro-cracks during heating and cooling. The thermal expansion coefficient of multi-wall CNT ranges from 16 to 26 $\times 10^{-6}°C^{-1}$ [33] and is even larger than that of HA and Ti6Al4V. But the CNT content (5–10 wt%) is relatively low and the effect of thermal expansion due to CNT is then less dominant. In addition, some interconnected micro-pores with size of 0.5 μm can be observed in the coatings at high magnification (Fig. 1a-ii–e-ii). Fewer and smaller micro-cracks are observed in nHA5TiO10CNT but micro-pores with similar size are still present. The specimen nHA10TiO5CNT with lower HA content (85 wt%) or higher TiO_2 content (10 wt%) possesses no micro-cracks, some micro-pores and smooth surface (Fig. 1e-i). Among HA, TiO_2 and CNT, the thermal expansion coefficient of TiO_2 ($9.0 \times 10^{-6}°C^{-1}$) is the most comparable to that of Ti6Al4V, resulting in minimizing the strain during heating and cooling. The TiO_2 nanoparticles dispersed uniformly between the HA crystals and CNTs causing an elimination of micro-cracks and micro-pores and an increase in density of the nanocomposite coating as schematically shown in Fig. 2. There are two functions of TiO_2 nanoparticles. Firstly, it acts a bonding agent for providing better adhesion bond to the oxide layer (rutile) of heated Ti6Al4V substrate. Secondly, its spherical shape can fill the gap between the needle-shape HA crystals and CNTs with large aspect ratio.

A typical cross-sectional appearance of nHA10TiO5CNT is shown in Fig. 3a. A continuous and uniform HA/TiO_2/CNT coating on the substrate can be observed. The thickness of all the coatings is about 7–10 μm. Thin HA coatings are more desirable while thick coatings obtained by plasma spraying have been reported to be prone to fracture and fragmentation during insertion and service [34]. From the compositional profile obtained from the coating to the substrate, a gradual decrease in Ca, P and C content and an increase of Ti content can be observed (Fig. 3b). The presence of Ca, P and C is probably from HA and CNTs in the coating. The combination of CNTs and TiO_2 enhances their mechanical and functional properties of the coatings, CNTs in the nanocomposite coatings act as reinforcement fibers to hold the matrix together, while TiO_2 acts as a filler to fill the voids between the HA and CNTs and provide good adhesion to the substrate resulting in fewer micro-cracks.

From the XRD patterns as shown in Fig. 4a and b, CNT and anatase remained unchanged (no decomposition or transformation) after heating at 800°C for an hour for simulating the sintering process. Anatase can only be transformed into rutile above 915°C [35]. The XRD patterns of monolithic HA and nanocomposite coatings after sintering at 800°C reveal high crystallinity (Fig. 4c–g). A high degree of crystallinity of HA would render the coating less susceptible to dissolution in body fluids [36, 37]. The distinct peaks for the nanocomposite coatings (nHA10TiO5CNT, nHA5TiO10CNT and nHA5TiO5CNT) such as anatase (25.324°), HA (25.879°) and rutile (27.435°) are apparently distinguishable, confirming their existence. No other crystalline phases such as α- and β-$Ca_3(PO_4)_2$ were observed in the XRD patterns. However, the existence of CNTs in the nanocomposite coatings cannot be confirmed by XRD because the peak at 26.3° of CNT may overlap with the peak at 25.879° of HA. In addition, the CNT content in

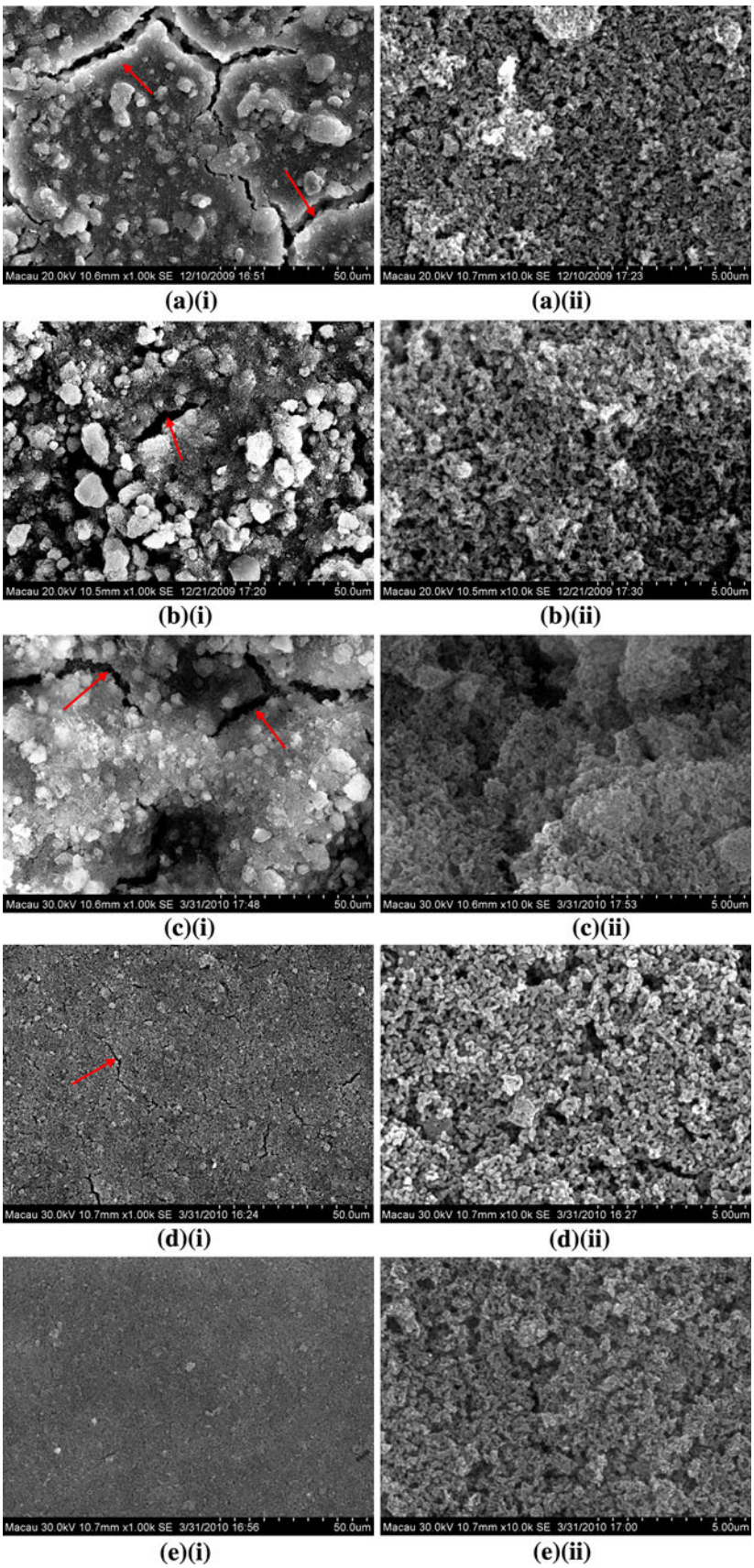

Fig. 1 SEM micrographs of various coated specimens after sintering: **a** nHA, **b** nHA10CNT, **c** nHA5TiO5CNT, **d** nHA5TiO10CNT, **e** nHA10TiO5CNT at different magnifications

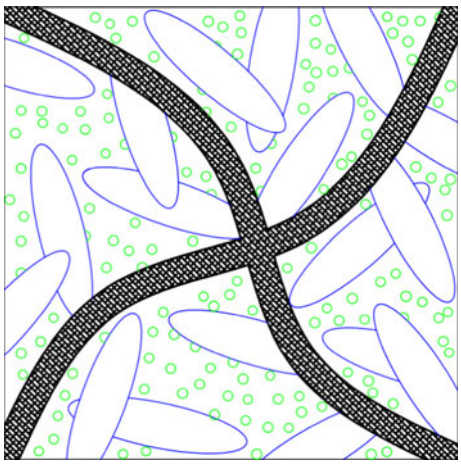

Fig. 2 Schematic diagram of structure of electrophoretically deposited HA/TiO_2/CNT nanocomposite layer (*strips*, *ellipses* and *circles* represent CNT, HA and anatase, respectively)

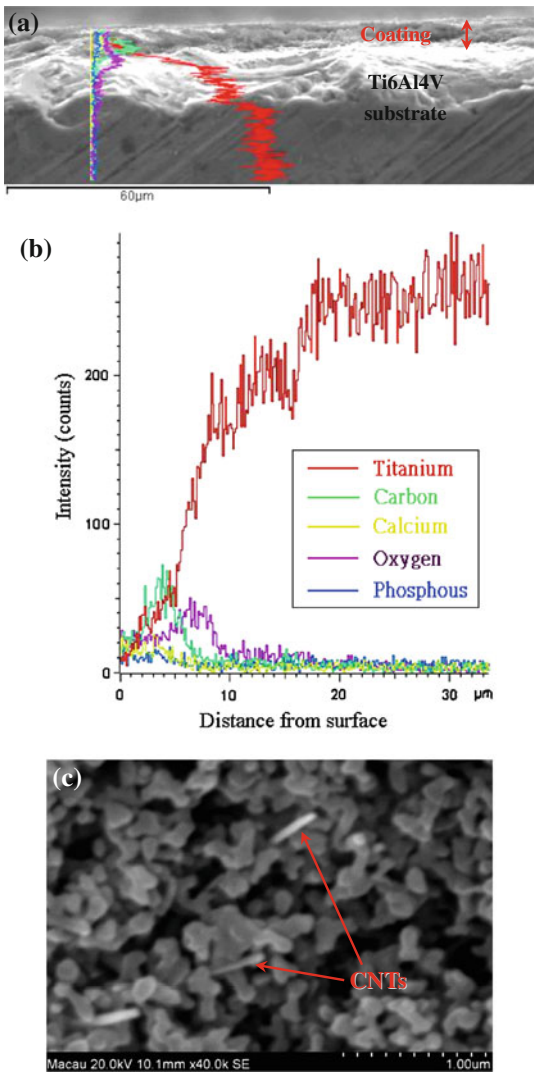

Fig. 3 **a** Cross-sectional view, **b** compositional profiles (by EDS line scan) from the coating to the substrate, **c** surface morphology of nHA10TiO5CNT

the nanocomposite coatings was relative low for XRD detection. However, the compositional profile of nHA10TiO5CNT (Fig. 3b) confirms the existence of carbon in such nanocomposite coating. The presence of CNTs in the specimen nHA10TiO5CNT is also evidenced by SEM micrograph as shown in Fig. 3c and similar observation was reported by Lin and his co-workers [17]. Increase in hardness of the HA/TiO_2/CNT coatings can also support the existence of the hard CNT (Table 1). Moreover, the diffraction peaks of rutile were detected in the XRD patterns of all coated specimens. This was formed due to thermal oxidation of the exposed substrate during sintering in the moderate vacuum atmosphere. It was reported that the rutile film was also an excellent interfacial bonding layer between Ti6Al4V substrate and HA coating [38]. The rutile interfacial layer can provide a ground to be attached by the anatase and HA in the nanocomposite coating.

3.2 Electrochemical corrosion behavior

Metallic implants may susceptible to corrosive attack by body fluids with subsequent release of metallic ions which might cause adverse effects to the surrounding tissues. It is crucial to understand the corrosion characteristics of implant materials interacting with physiological environment. The plot of *OCP* versus time and cyclic potentiodynamic polarization curves for the uncoated and coated specimens in Hanks' solution at 37°C are shown in Fig. 5. The values of steady *OCP* and I_{corr} are extracted as shown in Table 1. The *OCP* for various HA/TiO_2/CNT coatings (from −0.031 to 0.096 V) is much higher than that of the uncoated Ti6Al4V (−0.306 V). This shows higher thermodynamic stability of the HA/TiO_2/CNT coatings. It can be observed that the polarization curves of the coated specimens with HA/TiO_2/CNT shifted towards the region of lower current density and the nobler potential as compared with the uncoated Ti6Al4V. The I_{corr}, which represents the corrosion rate of metallic materials, achieves the minimum value for nHA10TiO5CNT (0.084 μA/cm^2) with 10 wt% TiO_2. The I_{corr} values of all nanocomposite coatings are in the range of 0.084–0.15 μA/cm^2 and are much lower than that of Ti6Al4V (8 μA/cm^2) and nHA (1.66 μA/cm^2). According to the values of I_{corr}, the corrosion resistance of the specimens is ranked as:

nHA10TiO5CNT > nHA5TiO10CNT > nHA5TiO5 CNT > nHA10CNT > nHA > Ti6Al4V

The corrosion resistance of nHA10TiO5CNT was higher than that of monolithic nHA and uncoated Ti6Al4V by factors of 20 and 95, respectively. This indicates that

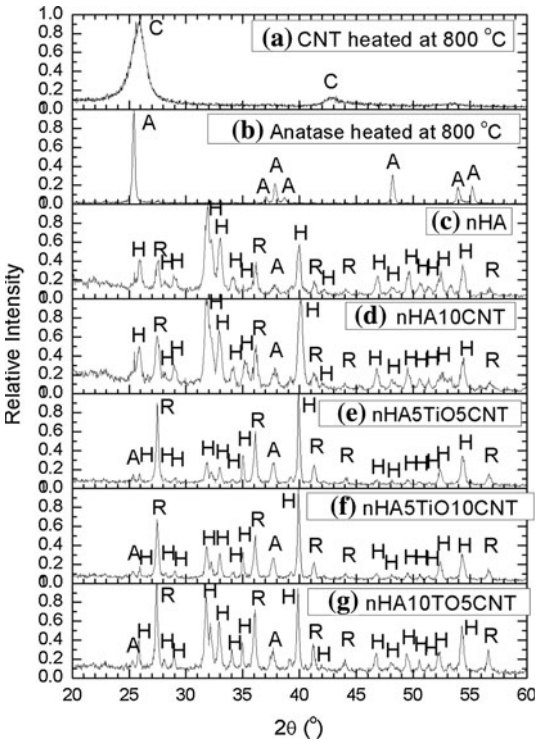

Fig. 4 XRD patterns of CNT, anatase and various coated specimens after sintering at 800°C for 1 h (*H* HA, *C* CNT, *A* Anatase, *R* Rutile)

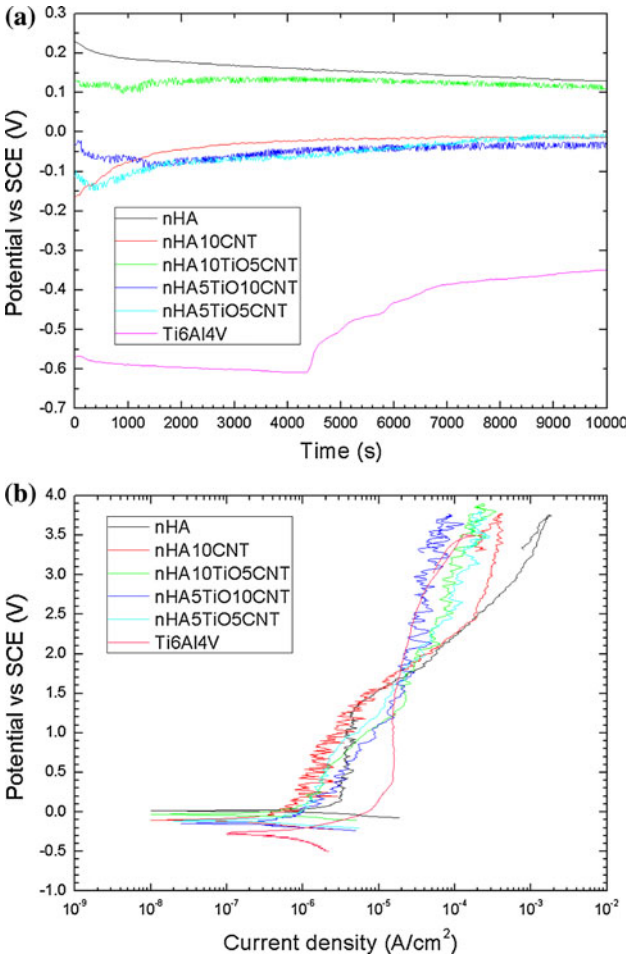

Fig. 5 **a** Plot of OCP versus time and **b** polarization curves of uncoated and coated specimens in Hanks' solution at 37°C

higher TiO_2 content helps to produce a coating with fewer micro-cracks. At potential below 1.7 V (Fig. 5b), all specimens coated with HA/TiO_2/CNT have significant improvement in corrosion resistance, the anodic current densities are lower than that of uncoated Ti6Al4V. Moreover, no specimen exhibits appreciable hysteresis loop indicating the absence of passivity breakdown.

In fact the corrosion resistance of coated metallic implants is greatly affected by the passivation ability of the metallic substrate and the quality of the coating. It was reported that the corrosion resistance of thermally oxidized Ti6Al4V was enhanced as compared with the air passivated Ti6Al4V due to presence of the rutile layer [39]. After sintering, the nanocomposite coating became more compact due to the clustering together of the nanoparticles and the rutile layer also formed below the coating. The coating acts as a barrier to the transport of electrons and ions between the substrate and the electrolyte, thus reducing the electrochemical reaction rate. The improved corrosion resistance of the Ti6Al4V coated with HA/TiO_2/CNT is attributed to the combined effect of the semi-insulating nanocomposite coatings and the rutile interlayer.

It was reported that the *OCP* of plasma sprayed HA coating on Ti6Al7Nb was more active, and the corrosion rate was higher compared with the substrate because of the presence of pores [40]. Although the nanocomposite HA/TiO_2/CNT coatings and monolithic HA coating formed by EPD also contained micro-pores, they are much smaller and less abundant than those formed in plasma spraying. Consequently, the nanocomposite coatings act as a semi-insulating barrier to lessen interaction of the solution and the Ti6Al4V substrate. When micro-pores are present in the nanocomposite coatings, conducting paths between the corrosive medium and the Ti6Al4V substrate will eventually be formed. Corrosion is associated with the penetration of chloride ion and water into the coating, transport of ions through the coating, and the subsequent electrochemical reactions at the interface of HA and Ti6Al4V. Zhang et al. [41] proposed that the corrosion mechanism of HA coating on Ti6Al4V with pores fabricated by EPD involved two steps. Firstly, hydrogen ions are produced at the interface area where corrosion of titanium occurs. It is then followed by the dissolution of HA in the high hydrogen ions concentration area. The local pH of the interface is very low because the hydrogen ions cannot be well circulated out of the interface and the dissolution of HA catalytically speeds up. Whenever the corrosion starts, it cannot stop until the

entire interfacial HA is dissolved. While anatase and CNT are chemical inert and do not interact with the corrosive medium. The coating then fails at the coating and substrate interfacial area [41]. The difference in corrosion resistance of various nanocomposite coatings on Ti6Al4V, which have different degrees of micro-pores and micro-cracks, is consistent with this corrosion mechanism.

3.3 Hardness and adhesion strength

The surface hardness and adhesion strength for various coated specimens are depicted in Table 1. The hardness of all nanocomposite coatings is higher than that of Ti6Al4V and monolithic HA coating mainly attributed to the hard CNT. Among the nanocomposite coatings, nHA10TiO5CNT possesses the highest hardness because the suitable TiO_2/CNT content makes the densified and crack-free coating despite of the lower CNT content (5 wt%). The hardness of nHA5TiO10CNT and nHA10CNT with the same CNT content (10 wt%) is similar but lower than that of nHA10TiO5CNT because of the presence of micro-cracks in the formers. Compared with the uncoated Ti6Al4V and monolithic HA coating, the hardness of nHA10TiO5CNT was increased by factors of 2.4 and 1.7, respectively. The high hardness of the HA coatings containing CNT on Ti6Al4V can improve their wear resistance and hence increase the service life of the load-bearing orthopedic implants. Lahiri and his coworkers reported that the addition of 4 wt% CNTs to HA plasma-sprayed coating improved the wear resistance by 80% and also resulted in less volume of debris generation [42] while the elastic modulus and fracture toughness increased by 72.5 and 350%, respectively.

All specimens coated with HA/TiO_2/CNT exhibit a higher adhesion strength (6.4–12.6 MPa) than that of the monolithic HA coating (5.9 MPa) and the plasma sprayed HA coating on titanium (4.5–6.8 MPa) [43]. The relative poor adhesion of plasma sprayed HA coating on Ti6Al4V mainly arise from the mismatch of their coefficients of thermal expansion [44]. The specimen nHA10TiO5CNT has the highest adhesion strength (12.6 MPa), this indicates that the adhesion strength increases with higher TiO_2 content. It was reported that CNTs can reduce the crack propagation in TiO_2/CNT films deposited by EPD [45] and mechanisms related to crack bridging and CNT pull-out are possible in these composite layers [46]. HA/TiO_2/CNT coatings showed higher adhesion strength to the Ti6Al4V substrate due to several possible reasons. Firstly, the mismatch of the coefficients of thermal expansion is reduced and the residual stress is prevented by the addition of spherical TiO_2 nanoparticles to the coating. Secondly, the cohesive strength between the different particles increases because chemical bonding of HA/TiO_2 on surface of CNTs may form during sintering [17]. Lastly, the dense HA/TiO_2/CNT coatings with reduced micro-cracks lead to higher adhesion strength.

The images of the fracture surfaces of nHA10TiO5CNT and nHA after adhesion strength tests are shown in Fig. 6. Failure occurred entirely at the interface for the nanocomposite coating nHA10TiO5CNT (Fig. 6a), adhesive failure is the main fracture mechanism. While some debris of the coatings remained on the surface of nHA shows both cohesive and adhesive failures (Fig. 6b). It suggests that the bond strength is dictated by the coating defects and the interface. Thus, the lower cohesive and adhesive strengths for nHA are attributed to the presence of high degree of micro-cracks.

3.4 In vitro bioactivity

The bioactivity of bioceramics has been defined as 'the bond ability with host bone tissue' [47]. This includes

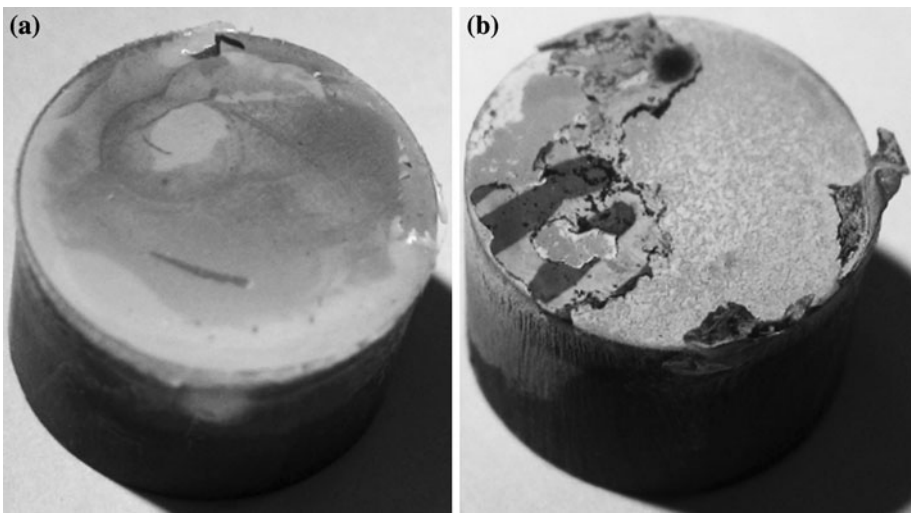

Fig. 6 Morphology of failed surface of (**a**) nHA10TiO5CNT and (**b**) nHA showing the coatings peeled off from the substrate after adhesion test

enhancing the ability of apatite formation, osteoblast differentiation and bone matrix formation. In order to develop new composite coatings for load-bearing orthopedic applications, it is vital to understand their bonding abilities to living bone. In the immersion test for evaluating in vitro bioactivity, the Hanks' solution used in the present study does not contain any biological matter such as bone-forming cells. Nevertheless, it has been pointed out in a recent review [48] that results of immersion tests in inorganic simulated body fluids like Hanks' solution are useful in predicting in vivo bone bioactivity. From Fig. 7, thick layers of apatite were formed on the surface of the monolithic HA and nanocomposite HA/CNT and HA/TiO_2/CNT coatings after immersion in Hanks' solution at 37°C for four weeks. Addition of TiO_2 and CNT in HA would not affect the apatite-forming ability on their surface. From Fig. 7b–f, the apatite particles on the coatings containing TiO_2 are observed to be smaller than those in nHA and nHA10CNT. According to the crystallization theory [49], in order for a stable apatite crystal to form, it requires to overcome the activation energy for crystallization. This energy is the result of the balance between the energy increase due to the formation of a new solid-solution interface and the energy decrease due to the crystal formation. For heterogeneous nucleation, i.e. nuclei are formed on a solid surface, the surface free energy between nucleus and solid must also be considered. Due to the presence of nano-size TiO_2 in the coatings, it is believed that surface free energy between nucleus and solid generally lower than the free energy per unit area of the nucleus-solution interface, so the critical size of the apatite particles is smaller and nucleation is easier [49]. By XRD analysis, the intensity of the apatite peaks in nHA10TiO5CNT after immersed in Hanks' solution for 4 weeks has found to be increased as shown in Fig. 8, confirming that the particles grown on the specimen are apatite. On contrary, no apatite was formed on the surface of Ti6Al4V (Fig. 7a). The present results reveal that the HA/TiO_2/CNT coatings formed by EPD are bone bioactive and hence favor osseointegration. However, the combination of simulated

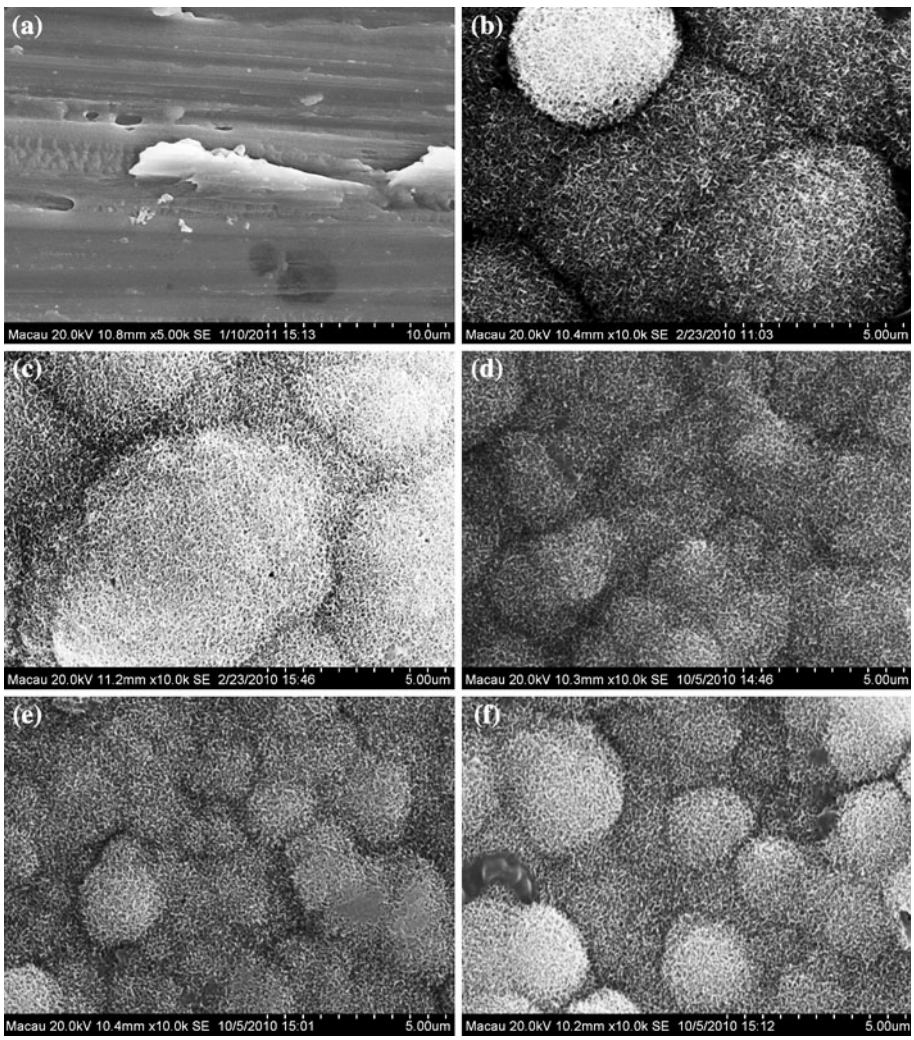

Fig. 7 SEM micrographs of uncoated and coated specimens after immersed in Hanks' solution for 4 weeks: **a** Ti6Al4V, **b** nHA, **c** nHA10CNT, **d** nHA10TiO5CNT, **e** nHA5TiO10CNT, **f** nHA5TiO5CNT

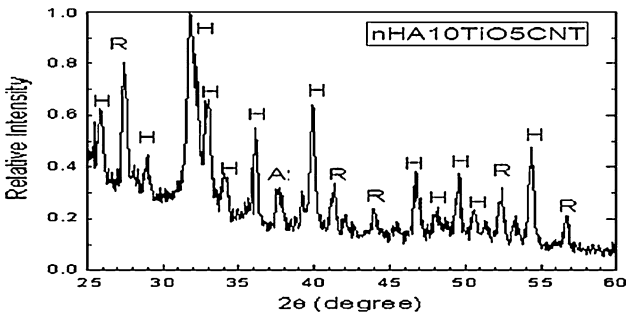

Fig. 8 Typical XRD pattern of nHA10TiO5CNT after immersed in Hanks' solution at 37°C for 4 weeks

body fluid and cell testing methods were recommended to evaluate the in vitro bioactivity of bioceramics, an approach which will improve the efficiency of screening bioceramics for further in vivo evaluation of bone repair and bone-forming [50]. So the further research should focus on the cell testing investigation of the nanocomposite coatings for future biomedical applications.

4 Conclusions

Nanocomposite HA/CNT/TiO_2 coatings with thickness of about 7–10 μm were successfully fabricated on Ti6Al4V by electrophoretic codeposition. All coated specimens show significant enhancement in corrosion resistance, hardness and adhesion strength. Among the specimens, the HA coating reinforced with 10% TiO_2 and 5% CNT (nHA10TiO5CNT) possessed the most uniform and the hardest surface (991 HV) without micro-crack, and the highest adhesion strength (12.6 MPa). The highest corrosion resistance was evidenced by a noble shift of open-circuit potential (0.096 V) and a lower corrosion current density (0.084 μA/cm^2). Formation of apatite particles on the surface of all HA/CNT/TiO_2 coatings after immersion in Hanks' solution at 37°C for 4 weeks indicates high bone bioactivity. Addition of TiO_2 and CNT in HA could markedly increase corrosion resistance, hardness and adhesion strength without compromising bioactivity.

Acknowledgments The work described in this paper was fully supported by a research grant from the Science and Technology Development Fund (FDCT) of Macau SAR (Grant no. 018/2007/A) and the Research Committee of University of Macau (Project no. RG064/06-07S/KCT/FST).

References

1. Long M, Rack HJ. Titanium alloys in total joint replacement—a materials science perspective. Biomaterials. 1998;19:1621–39.
2. Liu X, Chu PK, Ding C. Surface modification of titanium, titanium alloys, and related materials for biomedical applications. Mater Sci Eng. 2004;47:49–121.
3. Li TT, Lee JH, Kobayashi T, Aoki H. Hydroxyapatite coating by dipping method, and bone bonding strength. J Mater Sci Mater Med. 1996;7:355–7.
4. Chen J, Wolke JGC, de Groot H. Microstructure and crystallinity in hydroxyapatite coatings. Biomaterials. 1994;15:396–9.
5. Kay JF. Calcium phosphate coatings for dental implants: current status and future potential. Dent Clin North Am. 1992;36:1–18.
6. Eliaz N, Sridhar MT, Mudali UK, Raj B. Electrochemical and electrophoretic deposition of hydroxyapatite for orthopaedic applications. Surf Eng. 2005;21:238–42.
7. Lusquinos F, Pou J, Arias JL, Boutinguiza M, Leon B, Perez-Amor M. Alloying of hydroxyapatite onto Ti6Al4V by high power laser irradiation. J Mater Sci Mater Med. 2002;13:601–5.
8. Laxmidhar B, Meili L. A review on fundamentals and applications of electrophoretic depositions (EPD). Prog Mater Sci. 2000;52:1–61.
9. Wang C, Ma J, Cheng W, Zhang RF. Thick hydroxyapatite coating by electrophoretic deposition. Mater Lett. 2002;57:99–105.
10. Zheng XB, Ding CX. Characterization of plasma-sprayed hydroxyapatite/TiO_2 composite coatings. J Therm Spray Technol. 2000;9:520–5.
11. Wei M, Ruys AJ, Swain MV, Kim SH, Milthorpe BK. Interfacial bond strength of electrophoretically deposited hydroxyapatite coatings on metals. J Mater Sci. 1999;10:401–9.
12. Zhang EL, Yang K. Coating of calcium phosphate on biometallic materials by electrophoretic deposition. Trans Nonferrous Met Soc China. 2005;15:957–64.
13. Catledge SA, Fries M, Vohra YK. Nanostructured surface modification for biomedical implants. Encyclopedia of Nanoscience and Nanotechnology, vol. X, California: American Scientific Publishers; 2003. p.14.
14. Boccaccini AR, Cho J, Subhani T, Kaya C, Kaya F. Electrophoretic deposition of carbon nanotube-ceramic nanocomposites. J Eur Ceram Soc. 2010;30:1115–29.
15. Boccaccini AR, Keim S, Ma R, Li Y, Zhitomirsky I. Electrophoretic deposition of biomaterials. J R Soc Interface. 2010;7:S581–613.
16. Nieh TG, Wadsworth J. Hall-Petch relation in nanocrystalline solids. Scripta Met. 1991;25:955–8.
17. Lin C, Han H, Zhang F, Li A. Electrophoretic deposition of HA/MWNTs composite coating for biomaterial applications. J Mater Sci Mater Med. 2008;19:2569–74.
18. Kaya C. Electrophoretic deposition of carbon nanotube-reinforced hydroxyapatite bioactive layers on Ti–6Al–4 V alloys for biomedical applications. Ceram Int. 2008;34:1843–7.
19. Kaya C, Singh I, Boccaccini AR. Multi-walled carbon nanotube reinforced hydroxyapatite layers on Ti6AI4 V medical implants by electrophoretic deposition (EPD). Adv Eng Mater. 2008;10:1–8.
20. Kaya C, Kaya F, Cho J, Roether JA, Boccaccini AR. Carbon nanotube-reinforced hydroxyapatite coatings on metallic implants using electrophoretic deposition. Key Eng Mater. 2009;412:93–7.
21. Kwok CT, Wong PK, Cheng FT, Man HC. Characterization and corrosion behavior of hydroxyapatite coatings on Ti6Al4V fabricated by electrophoretic deposition. Appl Surf Sci. 2009;255:6736–44.
22. Bai Y, Neupane MP, Parks IS, Lee MH, Bae TS, Watari F, Uo M. Electrophoretic deposition of carbon nanotubes-hydroxyapatite nanocomposites on titanium substrate. Mater Sci Eng. 2010;30:1043–9.
23. Zhang B, Kwok CT, Cheng FT, Man HC. Fabrication of Nanostructured HA/CNT coatings on Ti6Al4V by electrophoretic deposition for biomedical applications. J Nanosci Nanotechnol. 2011 (In press).
24. Albayrank O, El-Atwani O, Altintas S. Hydroxyapatite coating on titanium substrate by electrophoretic deposition method: effects

of titanium dioxide inner layer on adhesion strength and hydroxyapatite decomposition. Surf Coat Technol. 2008;202: 2482–7.
25. Bae JC, Yoon YJ, Lee SJ, Baik HK. Field emission properties of carbon nanotubes deposited by electrophoresis. Phys B. 2002; 323:168–70.
26. Mondragon-Cortez P, Vargas-Gutierrez G. Electrophoretic deposition of hydroxyapatite submicron particles at high voltages. Mater Lett. 2004;58:1336–9.
27. Cho J, Schaab S, Roether JA, Boccaccini AR. Nanostructured carbon nanotube/TiO_2 composite coatings using electrophoretic deposition (EPD). J Nanopart Res. 2008;10:99–105.
28. Gomez-Vega JM, Saiz E, Tomsia AP. Glass-based coating for titanium implant alloys. J Biomed Mater Res. 1999;46:549–59.
29. Berndt CC, Haddad GN, Farmer AJD, Gross KA. Thermal spraying for bioceramic applications. Metals Forum. 1990;14: 161–73.
30. ASTM Standard G61-94, Conducting cyclic potentiodynamic polarization measurements for localized corrosion susceptibility in iron-, nickel-, or cobalt-based alloys, ASTM Standards, ASTM, PA, USA (1994).
31. International Standard ISO 13779-4, Implants for surgery–Hydroxyapatite–Part 4: Determination of coating adhesion strength; 2002.
32. Wei M, Ruys AJ, Milthorpe BK, Sorrell CC. Precipitation of hydroxyapatite nano-particle: effects of precipitation method on electrophoretic deposition. J Mater Sci. 2005;16:319–24.
33. Yutaka M, Ryuji F, Hiroshi K, Hideki T, Eiji N, Masaki T, Makoto S, Akihiko F, Xinluo Z, Sumio I, Yoshinori A. Multiwalled carbon nanotubes grown in hydrogen atmosphere: an X-ray diffraction study. Phys Rev B. 2001;64:0731051.
34. Contu F, Elsener B, Hohni H. Characterization of implant materials in fetal bovine serum and sodium sulfate by electrochemical impedance spectroscopy, I: mechanically polished samples. J Biomed Mater Res. 2002;62:412–21.
35. Hugh C, editor. Encyclopedia Britannica. 11th ed. UK: Cambridge University Press; 1911.
36. Sarkar P, Nicholson PS. Electrophoretic deposition (EPD): mechanisms, kinetics, and application to ceramics. J Am Ceram Soc. 1996;79:1987–2002.
37. Mizutani T, Uchida S, Fujishiro Y, Sato Y. Synthesis of monodispersed hydroxyapatite using calcium polyphosphate gels as precursors. Br Ceram Trans. 1998;97:105–11.
38. Nie X, Leyland A, Matthews A. Deposition of layered bioceramic hydroxyapatite/TiO_2 coatings on titanium alloys using a hybrid technique of micro-arc oxidation and electrophoresis. Surf Coat Technol. 2000;125:407–14.
39. Narayanan R, Seshadri SK. Synthesis and corrosion of functionally gradient TiO_2 and hydroxyapatite coatings on Ti–6Al–4 V. Mater Chem Phys. 2007;106:406–11.
40. Lavos-Valereto IC, Costa I, Wolynec S. The electrochemical behavior of Ti-6Al-7Nb alloy with and without plasma-sprayed hydroxyapatite coating in Hanks' solution. J Biomed Mater Res. 2002;63:664–70.
41. Zhang Z, Dunn MF, Xiao TD, Tomsia AP, Saiz E. Nanostructured hydroxyapatite coatings for improved adhesion and corrosion resistance for medical implants. Nanotech and Biotech Convergence, Stamford: Stamford; 6–7 May 2002. p. 291–296.
42. Lahiri D, Benaduce AP, Rouzaud F, Solomon J, Keshri AK, Kos L, Agarwal A. Wear behavior and in vitro cytotoxicity of wear debris generated from hydroxyapatite–carbon nanotube composite coating. J Biomed Mater Res. 2011;96:1–12.
43. Oh I, Nomura N, Chiba A, Murayama Y, Masahashi N, Lee B, Hanada S. Microstructures and bond strengths of plasma-sprayed hydroxyapatite coatings on porous titanium substrates. J Mater Sci Mater Med. 2005;16:635–40.
44. Himann RB, Kurzweg H, Vu TA. Hydroxyapatite-bond coat systems for improved mechanical and biological performance of hip implants. In: Proceedings of the 15th International Thermal Spray Conference, France, 1998; p. 999–1005.
45. Jarernboon W, Pimanpang S, Maensiri S, Swatsitang E, Amornkitbamrung V. Effects of multiwall carbon nanotubes in reducing microcrack formation on electrophoretically deposited TiO_2 film. J Alloy Compd. 2009;476:840–6. doi:10.1016/j.jallcom.2008.09.157.
46. Cho J, Boccaccini AR, Shaffer MSP. Ceramic matrix composites containing carbon nanotubes. J Mater Sci. 2009;44:1934–51.
47. Hench LL. Bioceramics: from concept to clinic. J Am Ceram Soc. 1991;74:1487–510. doi:10.1111/j.1151-2916.1991.tb07132.x.
48. Kokubo T, Takadama H. How useful is SBF in predicting in vivo bone bioactivity? Biomaterials. 2006;27:2907–15.
49. Bohner M, Lemaitre J. Can bioactivity be tested in vitro with SBF solution? Biomaterials. 2009;30:2175–9.
50. Wu C, Xiao Y. Evaluation of the in vitro bioactivity of bioceramics. Bone Tissue Regen Insights. 2010;3:1–4.